UNIVERSITÄT AUGSBURG
Universitätsbibliothek

OPEN ACCESS
OPUS AUGSBURG

Effect of host anisotropy on phosphorescent emitter orientation and light outcoupling in OLEDs

Bình Minh Nguyễn, Jonas Kröber, Philipp Schütz, Klaus Ruhland, Falk May, Wolfgang Brütting

Angaben zur Veröffentlichung / Publication details:

Nguyễn, Bình-Minh, Jonas Kröber, Philipp Schütz, Klaus Ruhland, Falk May, and Wolfgang Brütting. 2026. "Effect of host anisotropy on phosphorescent emitter orientation and light outcoupling in OLEDs." *Advanced Optical Materials* 14 (8): e00002. https://doi.org/10.1002/adom.202600002.

Nutzungsbedingungen / Terms of use:

CC BY 4.0

Dieses Dokument wird unter folgenden Bedingungen zur Verfügung gestellt: / This document is made available under these conditions:
CC-BY 4.0: Creative Commons: Namensnennung
Weitere Informationen finden Sie unter: / For more information see:
https://creativecommons.org/licenses/by/4.0/deed.de

Check for updates

Advanced Optical Materials

ADVANCED OPTICAL MATERIALS
www.advopticalmat.de

RESEARCH ARTICLE OPEN ACCESS

Effect of Host Anisotropy on Phosphorescent Emitter Orientation and Light Outcoupling in OLEDs

Bình-Minh Nguyễn[1] | Jonas Kröber[2] | Philipp Schütz[2] | Klaus Ruhland[1] | Falk May[2] | Wolfgang Brütting[1]

[1]Institute of Physics, University of Augsburg, Augsburg, Germany | [2]Merck KGaA, Darmstadt, Germany

Correspondence: Wolfgang Brütting (wolfgang.bruetting@physik.uni-augsburg.de)

Received: 22 October 2025 | **Revised:** 8 January 2026 | **Accepted:** 19 January 2026

Keywords: emitter orientation | guest-host system | light outcoupling | OLEDs | optical anisotropy

ABSTRACT

Preferential alignment of the emitting molecules' transition dipole moments (TDMs) is an established method to boost light outcoupling from organic light–emitting diodes (OLEDs). Key factors to achieve this are shape and/or chemical anisotropy of the emitter itself, and the glass transition temperature of the host in light–emitting guest-host systems, if the layers in the OLED are prepared by vacuum deposition. Here we demonstrate that the optical anisotropy of the host material plays a decisive role for tuning the orientation of phosphorescent emitters as well. We find that the TDM orientation of a cage-like metal–organic Iridium complex, which is derived from the well-known $Ir(ppy)_3$, is correlated with the orientation order parameter S of the host material (and its birefringence Δn). Specifically, strong horizontal TDM alignment is achieved for lying host molecules having negative S (and Δn). However, the actual increase in OLED efficiency by a more horizontal emitter orientation is less than expected. This can be explained by the effect of birefringence of the emission layer on optical wave propagation and the coupling to lossy modes in an OLED. Furthermore, since the used (co)host materials are two-component mixtures of electron- respectively hole-transporting species, the balance between both and its impact on the location of the emission zone are critical as well. Overall, we present a comprehensive treatment of the different effects of host anisotropy on the efficiency of OLEDs.

1 | Introduction

Organic light–emitting diodes (OLEDs) are the most prominent example for the success of organic semiconductors in optoelectronics. They are well established in commercial applications, specifically as flat-panel displays used in mobile smartphones or high-definition television screens [1–3]. Using phosphorescent emitter molecules (in the red to green spectral region), they can reach an internal quantum efficiency (IQE) for the conversion of charge carriers to photons close to 100% [4]. However, a major fraction of them is trapped inside the device due to total internal reflection and other optical losses, like wave-guided modes or surface plasmons (see e.g. in Ref. [5]). A simple, and yet very powerful, approach to extract more light from these multi-layer structures is to align the optical transition dipole moments (TDMs) of the emitter molecules preferentially in the film plane [6–8]. It does not require expensive micro-structuring of the active layers or the substrate [9] and can even be combined with some of these methods to give a boost of the fraction of outcoupled light by up to 50% relative to the case of random TDM orientation [10, 11].

Regarding the driving forces behind emitter alignment, several factors have already been identified to be responsible for achieving horizontal TDM orientation in emissive guest-host systems prepared by physical vapor deposition (see e.g. [12] for an overview). First, and foremost, the shape of the emitter molecule itself plays a key role, with rod- or disc-like molecules having an intrinsic tendency to lie down on the surface of an evaporated film [13]. While this was originally demonstrated in

This is an open access article under the terms of the Creative Commons Attribution License, which permits use, distribution and reproduction in any medium, provided the original work is properly cited.

© 2026 The Author(s). *Advanced Optical Materials* published by Wiley-VCH GmbH

single-component neat films of fluorescent materials only, it also holds in co-evaporated guest-host (G-H) systems – at least qualitatively [6]. However, even some heteroleptic phosphorescent emitters showed anisotropic light emission, although they were long considered to be almost spherical [7]. Additionally, in case of such G-H systems, the glass transition temperature of the host material was identified as another key parameter to control the alignment of emissive fluorescent molecules [14]. While this was later on confirmed for thermally activated delayed fluorescence (TADF) emitters as well [15], the original work of Mayr et al. did not find such a trend for phosphorescent emitters, like the well known $Ir(ppy)_3$ or $Ir(ppy)_2(acac)$ [14].

Nevertheless, these metal–organic Iridium complexes are currently the dominant emitter species in green and red OLED pixels for commercial applications, and there are attempts to commercialize blue phosphorescent emitters [16], although several other approaches to blue exist as well [17–19]. Regardless which of them will in the end be successful, the advantage of aligned emissive TDMs is valid in all cases. Thus, detailed knowledge of the alignment mechanism is of paramount importance.

Early on, the chemical structure with (up to) three organic ligands surrounding the central Ir atom was considered to be the main factor for determining their TDM orientation. Specifically, it was found that the homoleptic complex $Ir(ppy)_3$ with three identical phenylpyridine (ppy) ligands exhibits random orientation in G-H systems consisting of typically up to 10% of the emitter doped in a wide-gap (often carbazole-based) host, while the heteroleptic analogue $Ir(ppy)_2(acac)$, where one of the ppy ligands is replaced by a non-emissive acac ligand, shows a more horizontal orientation [20]. This was explained later on by the chemical asymmetry of these molecules, which drives the non-emissive acac ligand to orient toward the free surface of the growing film [21]. And, since the TDM vectors of the two emissive ppy ligands are perpendicular to the axis through the acac ligand (the molecule's $C2$ pseudosymmetry axis), preferentially horizontal alignment of them is achieved. In the case of $Ir(ppy)_3$, the three ppy ligands are equivalent and their TDM vectors lie almost in one plane, but the molecule itself does not have a preferred "landing orientation" on the film surface. Note that pronounced alignment of such emitter molecules is only achieved by physical vapor deposition, while solution processing – like e.g. spin-coating – leads to more or less isotropic emitter orientation [22, 23].

Later studies have revealed that the degree of horizontal alignment can be tuned by chemically modifying the ligands, both in heteroleptic as well as homoleptic complexes. For example, Kim et al. have proposed to use the electrostatic surface potential maps of the complexes, and correlated them to alignment [24–27], while Jung et al. [28], Schmid et al. [29] and Kim et al. [30, 31] showed that by tuning the shape anisotropy, even homoleptic complexes can exhibit a substantial degree of non-isotropic alignment, which is favorable for improving light outcoupling from OLEDs.

However, in most of these studies, the role of the host material has achieved far less attention than the design of the emitter molecules. Nevertheless, in some cases, an influence of the host material on the emissive TDM orientation of Ir complexes was reported, but the given explanation was rather generic as some kind of intermolecular interaction [32]. More systematically, in the work by Huh et al., a correlation between the emissive TDM orientation of a disc-like Pt complex (PtOEP) and the nematic order parameter S of the host materials, as obtained from the optically anisotropic absorption coefficient of the films, was observed [33]. Thereby, the S parameter was obtained by spectroscopic ellipsometry from the difference in the ordinary (in-plane) and extraordinary (out-of-plane) component of the extinction coefficient in the ultra-violet spectral range, while the emission occurred in the red region. They found a strong correlation between the S parameters of the different host materials and the resulting alignment of the emitter in the respective host. In another study, they investigated the dependence of the alignment of several Ir complexes on the glass transition temperature of the host materials [34]. Surprisingly, higher T_g-hosts yielded less horizontal TDM alignment – contrary to what was observed in fluorescent emitters.

Other groups, studied orientation effects in TADF emitters by controlling alignment of the host material [35]. They found that alignment of a host material, like TCTA with its strong tendency to develop optical anisotropy (i.e. birefringence), can boost emitter alignment as well. And in another study by the same group, they used mixtures of two different cohost materials with either electron or hole transporting properties to manipulate the emissive TDM of a TADF emitter [36]. In this case, they focused particularly on the glass transition temperature of the host materials and suggested that at least one of them should have a high T_g to achieve the preferred horizontal TDM orientation.

This short (and by far not comprehensive) review of literature shows that the host material in an emissive G-H system plays a key role for tuning the emissive TDM orientation. However, for the important class of phosphorescent Ir-based OLED emitters, there is still a lack of a clear picture of the role of host materials for tuning their TDM alignment, which is of central importance for light outcoupling, and the resulting efficiency of OLEDs.

2 | Materials and Basic Approach

Complementary to our previous work [37], where we tuned the TDM orientation by changing the chemical structure of a series of Iridium emitter complexes and deposited them in a given host material, here we use *one and the same* Ir emitter complex (see Figure 1) and co-evaporate it with different host materials. Specifically, we use cohost matrices consisting of an electron- and a hole-transporting species, and tune their optical anisotropy by varying the mixing ratio of suitable e-/h-type components. The studied heteroleptic yellow phosphorescent Ir complex is derived from the prototypical emitter $Ir(ppy)_3$ and is described in patents [38, 39]. For details of the synthesis and chemical characterization see Section S1.

As shown in Figure 1a, the structure consists of a facial $Ir(ppy)_3$ core, where all three ppy ligands are extended by one additional phenyl ring each, which are covalently bridged via another central phenyl ring in a cage-type fashion. Additionally, one of the original ppy ligands is elongated at the pyridin side by two para-connected phenyl rings, which makes this ligand the emissive one and shifts the emission color to the yellow spectral region. From density functional theory calculations (see e.g. in Ref.[37]), we

21951071, 2026, 8, Downloaded from https://advanced.onlinelibrary.wiley.com/doi/10.1002/adom.202600902 by Open Access University of Augsburg - Universitätsbibliothek Augsburg , Wiley Online Library on [23/02/2026]. See the Terms and Conditions (https://onlinelibrary.wiley.com/terms-and-conditions) on Wiley Online Library for rules of use; OA articles are governed by the applicable Creative Commons License

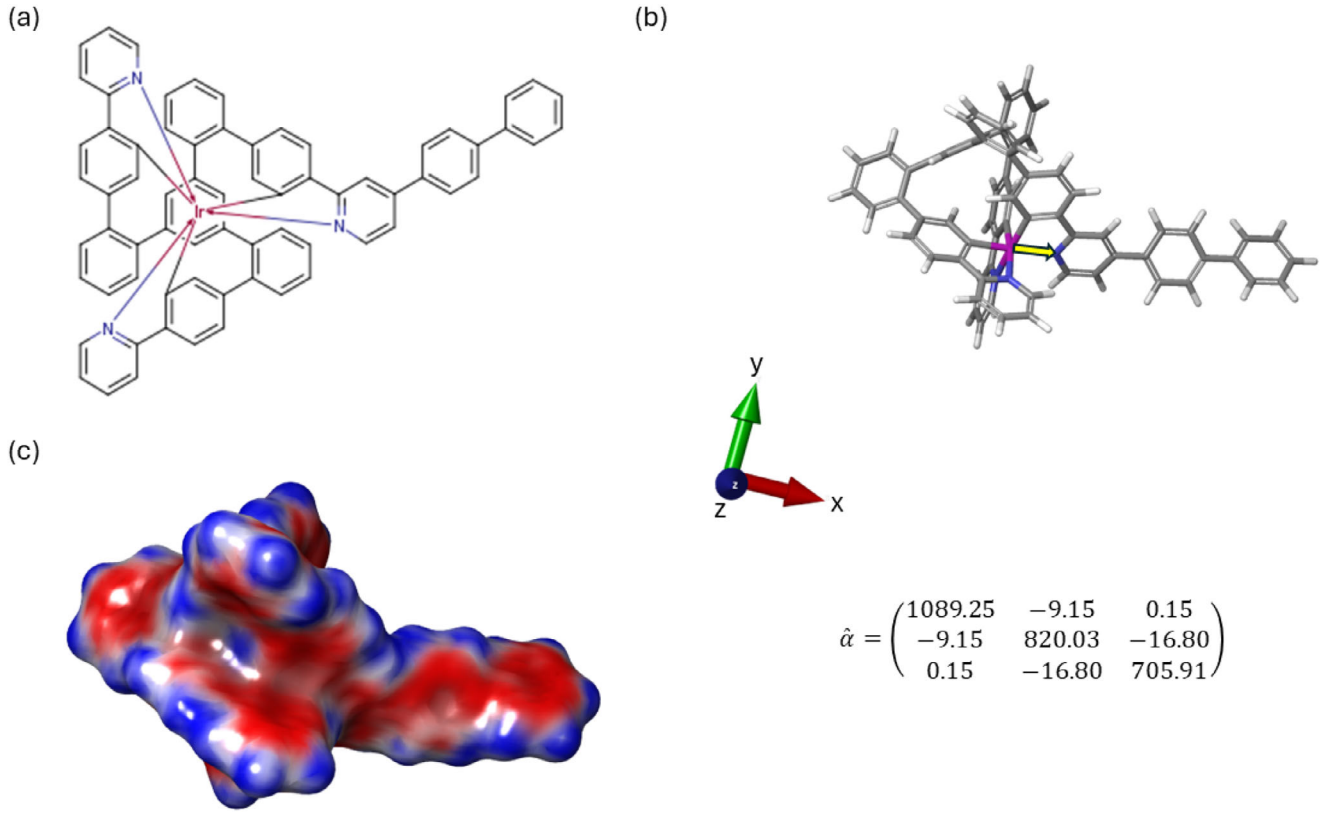

FIGURE 1 | (a) 2D and (b) 3D structures of the cage-type yellow Ir(ppy)$_3$-derivative emitter used in this work. A phenyl ring (sitting above the Iridium atom in the center) bridges all three sub-ligands by covalent bonds. The TDM vector (shown in yellow) points from the central Iridium atom toward the Nitrogen atom of the emissive ligand. (c) Map of the electrostatic surface potential (blue: positive, red: negative) on the emitter molecule. $\tilde{\alpha}$ is the polarizability tensor (in atomic units) relative to the given coordinate system, which is identically used for the 3D structure shown in (b) and the ESP map in (c). Note that the TDM vector is not exactly collinear with the x-axis, but includes a small angle of about 9° with it.

obtain the transition dipole moment vector of the lowest triplet T_1 to ground state S_0 transition that points from the Ir atom in the center of the complex toward the nitrogen atom of the emissive ligand, Figure 1b. Note that, strictly speaking the ligand sphere counts as just *one* ligand, since all three sub-ligands are covalently linked together via a phenyl ring,

As host materials, we chose compounds with high enough T_1 energy. These host materials are co-evaporated (together with the emitter) in different ratios to vary the resulting optical and electronic properties of the cohost system. Typically, one component of such cohost matrices is an electron transporting ("e-type") species, while the other is hole transporting ("h-type"). By mixing two such species with different birefringence (Δn) via co-evaporation, cohost systems with tunable Δn values can be obtained. Prototypical materials are triazines as e-type and biscarbazoles as h-type components, respectively. Overall, 25 different cohost systems were prepared – covering a range in Δn between about –0.3 and +0.1 (see Table S1 for the full list). These cohost matrices were doped with 8–12% of the yellow phosphorescent emitter by simultaneous triple evaporation of all compounds in high vacuum, resulting in emissive thin films that were used for optical characterization and, thereafter, also tested in OLEDs.

As exemplary combination, we have used T2T (2,4,6-Tris(biphenyl-3-yl)-1,3,5-triazine, Figure 2a) being e-type with $\Delta n \approx +0.14$ and $T_g \approx 57$°C, indicating preferentially standing molecules, and BCzPh (9,9'-Diphenyl-9H,9'H-3,3'-bicarbazole, Figure 2b) being h-type with $\Delta n \approx -0.04$, i.e. almost random orientation of molecules, and $T_g \approx 98$°C. These two cohosts were used in device 4 at an h/e-ratio ($c_h/(c_e + c_h)$) of 34%, resulting in a slightly positive $\Delta n \approx 0.015$ and an effective $T_g \approx 72$°C. Another cohost pair was the triazine derivative 3-[3-[9-(4,6-Diphenyl-1,3,5-triazin-2-yl)-2-dibenzofuranyl]phenyl]-9-phenyl-9H-carbazole (Figure 2c, $\Delta n \approx -0.11$, $T_g \approx 125$°C) and the biscarbozole 9-[1,1'-Biphenyl]-3-yl-9'-[1,1'-biphenyl]-4-yl-3,3'-bi-9H-carbazole (Figure 2d, $\Delta n \approx -0.13$, $T_g \approx 119$°C). They were used in device 21 at an h/e-ratio of 67%, resulting in overall negative $\Delta n \approx -0.145$ and a higher effective $T_g \approx 124$°C. Other used cohosts contained Merck-internal materials with preferential electron or hole transporting properties, respectively, so that ambipolar transport in the cohost systems with tunable birefringence was obtained.

First, the optical anisotropy of the films was determined by variable-angle spectroscopic ellipsometry (VASE) as described, e.g., in Ref. [13]. This concerns the optical dielectric function and, specifically, the wavelength-dependent refractive index $n(\lambda)$ as well as the extinction coefficient $\kappa(\lambda)$ and their anisotropy with respect to the substrate normal, i.e. their ordinary components (n_o, κ_o) in the film plane vs. their extraordinary components (n_e, κ_e) perpendicular to it. Note that we assume only uniaxial anisotropy here, because the deposited films are non-crystalline and do not have any preferential alignment within the substrate

21951071, 2026, 8, Downloaded from https://advanced.onlinelibrary.wiley.com/doi/10.1002/adom.202600902 by Open Access University of Augsburg - Universitatsbibliothek Augsburg , Wiley Online Library on [23/02/2026]. See the Terms and Conditions (https://onlinelibrary.wiley.com/terms-and-conditions) on Wiley Online Library for rules of use; OA articles are governed by the applicable Creative Commons License

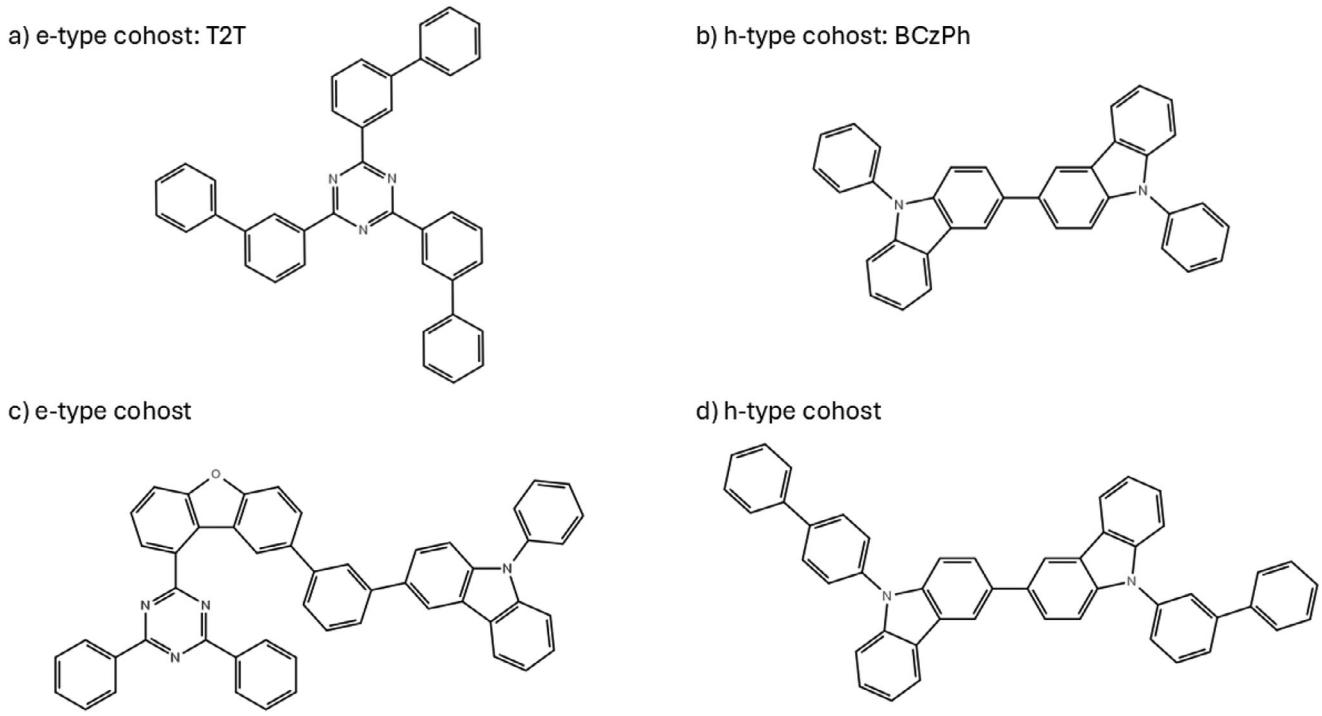

FIGURE 2 | Exemplary structures of cohosts used in this work. (a) e-type 2,4,6-Tris(biphenyl-3-yl)-1,3,5-triazine (T2T) and (b) h-type 9,9'-Diphenyl-9H,9'H-3,3'-bicarbazole (BCzPh) are used in device 4; (c) e-type 3-[3-[9-(4,6-Diphenyl-1,3,5-triazin-2-yl)-2-dibenzofuranyl]phenyl]-9-phenyl-9H-carbazole and (d) h-type 9-[1,1'-Biphenyl]-3-yl-9'-[1,1'-biphenyl]-4-yl-3,3'-bi-9H-carbazole are used in device 21.

plane. Following standard conventions, birefringence Δn and the nematic order parameter S are defined as follows:

$$\Delta n := n_e - n_o \quad \text{and} \quad S := \frac{\kappa_e^{\max} - \kappa_o^{\max}}{\kappa_e^{\max} + 2\kappa_o^{\max}} \tag{1}$$

Both are – a priori – wavelength dependent, but it is common to take Δn in the non-resonant region below the energy gap of the materials, i.e. at longer wavelength, whereas S is determined from the absorption peak corresponding to the gap. Specifically, we take Δn at the emission peak wavelength (≈570 nm) of the yellow emitter and S in the range of cohost absorption below 400 nm.

In principle, the determination of the optical constants $n(\lambda)$ and $\kappa(\lambda)$ of material mixtures can follow different approaches. One is an effective-medium approach (EMA), which uses the known optical constants of the neat constituents and calculates an *effective* value as a weighted average of them. An often used EMA, is the Maxwell–Garnett expression for the calculation of the effective (complex) permittivity $\varepsilon(\lambda)$ in the visible optical range according to [40]:

$$\varepsilon_{\text{eff}} = \varepsilon_1 \frac{1 + 2f\frac{\varepsilon_2 - \varepsilon_1}{\varepsilon_2 + 2\varepsilon_1}}{1 - f\frac{\varepsilon_2 - \varepsilon_1}{\varepsilon_2 + 2\varepsilon_1}} \tag{2}$$

Therein, ε_{eff} is the effective permittivity of the mixture, ε_1 and ε_2 are the corresponding values of the neat components, whereby component one is assumed to be the dominant species, and f is the fraction of the less abundant species, i.e. component two. The calculation of the optical constants n and κ from ε_{eff} is then straightforward. This approach is fast, as it only requires explicit measurement of the two neat species in a mixing series, but it neglects possible interactions between both that might lead to deviations from the expected trend. Specifically, if a molecular species with positive birefringence (standing molecules) is mixed with another one having negative birefringence (lying molecules), it is not clear if alignment in the codeposited film is just a weighted average of both, or if film growth exhibits a different tendency upon mixing them.

Therefore, we have followed a different approach and have investigated all the prepared cohost mixtures separately by VASE to determine their specific optical constants (and the corresponding Δn values and S parameters) — see Figures S3–S7, for a complete survey of the host materials' data sets. We also want to note that – strictly speaking – the additional 8–12% emitter doping would also contribute to the optical constants of the final emissive guest-host system. However, since the emitter doping concentration is low and very similar in all 25 samples, we did not take this additional contribution into account and used Δn and S parameters of the cohost only. Nevertheless, in some exemplary cases we explicitly measured (n, κ) data of samples without and with emitter and compared them to an EMA model of the cohost plus emitter system to verify that the emitter is negligible for the overall S or Δn values. Further, since the cohost matrices have varying ratios of e- and h-type host components, the wavelength of the dominant maximum in the extinction coefficient that will be used for the determination of the cohost's S parameter can vary by about 25–30 nm with the mixing ratio. For this reason, we used a weighted average value of the S parameters of both cohost species (e-/h-type); see Supporting Information for further details. However, we also checked that this does not have a significant impact on the results of our analysis.

21951071, 2026, 8, Downloaded from https://advanced.onlinelibrary.wiley.com/doi/10.1002/adom.202600902 by Open Access University of Augsburg - Universitätsbibliothek Augsburg , Wiley Online Library on [23/02/2026]. See the Terms and Conditions (https://onlinelibrary.wiley.com/terms-and-conditions) on Wiley Online Library for rules of use; OA articles are governed by the applicable Creative Commons License

Another property that is reported to affect the alignment of emitter molecules in a guest-host system, is the glass transition temperature T_g of the host material. Again, for the mixed cohost systems under consideration here, we have to use an *effective* T_g derived from the so-called Fox equation ([41]):

$$\frac{1}{T_{g,\mathrm{eff}}} = \frac{c_1}{T_{g,1}} + \frac{c_2}{T_{g,2}} \tag{3}$$

where $c_{1(2)}$ and $T_{g,1(2)}$ are the respective weight fractions and T_g's of the two cohost constituents. Strictly speaking, the emitter itself would also contribute to the effective T_g, but since its content is low and its T_g is not exactly known (but it is estimated to be rather high at about 370°C), we neglect it here as well.

A compilation of the relevant material parameters (Δn, S, $T_{g,\mathrm{eff}}$) of all 25 cohost systems is presented in Table S1.

3 | Results and Discussion

Regarding orientation trends in Ir-based phosphorescent emitters, the traditional approach has been to use ancillary ligands and chemically modify both emissive and/or ancillary ligands, e.g., by substitution with different functional groups in order to change properties like their aspect ratio or electrostatic surface potential (ESP) [24–27]. In that case, knowledge about the chemical structures of the emitter and the host is essential, as well as details of their electronic properties and packing in the film, which may require time consuming computational studies. Here, we follow a different approach, as we have one and the same emitter doped in a series of cohost materials, where details of the chemical structures of the latter do not matter. Instead, we use a simple macroscopic observable, namely the optical anisotropy of the host and correlate it with the measured emitter orientation. This is motivated by the fact that, at least in the absence of strong chemical asymmetries or ancillary ligands on the emitter, the underlying mechanism for emitter orientation is based on van der Waals interactions or, more precisely, London dispersion forces – and not on Coulomb interactions (weighted by the ESP-derived partial charges on the surface of emitter complexes and host materials), as was shown recently by Kim et al. [30].

As already explained in the original work by London [42], such dispersion forces are the main contribution to van der Waals forces in larger molecules, even if they have a permanent dipole moment. Essentially, the interaction strength U is proportional to the square of their electronic polarizability α and scales with the 6th power of the reciprocal distance between them ($U \propto \alpha^2/R^6$). However, except for simple gases, the polarizability is not just a scalar number but a tensor with three (different) eigenvalues. Thus, the London dispersion interaction between molecules of anisotropic shape (and polarizability) is anisotropic in itself. This has nicely been demonstrated with n-alkanes in the early work of Fowkes, where they showed correlated molecular orientation of long-chain alkanes in the liquid phase owing to "an enhancement in the London dispersion forces between pairs of parallel molecules because of the much greater polarizability parallel to the chains" [43].

For the Ir emitter complex studied here, there is no pronounced anisotropy in its ESP (see Figure 1c), but it has an anisotropic shape and, thus, an anisotropic polarizability tensor ($\tilde{\alpha}$) with eigenvalues differing roughly by 40%. And, the largest eigenvalue is observed in the direction of the emissive ligand (see Figure 1). Thus, our key hypothesis is that – in the absence of other strong aligning factors like, e.g., ancillary ligands – the alignment of the studied emitter molecule is driven by anisotropic London dispersion interactions with the host, which can be modified by changing the direction and magnitude of the host's optical birefringence in thin films (or its S parameter).

3.1 | Emitter Orientation in Evaporated Films

For studying correlations between the cohost properties and the emissive dipole orientation of the used yellow phosphorescent Ir complex, we prepared G-H systems of 8–12% emitter-doped films on fused silica substrates and studied their angular dependent photoluminescence (ADPL), which is an established technique to determine emitter orientation [44, 45]. With the knowledge of the cohost's optical constants (and its birefringence), we are able to extract an orientation parameter Θ from wave-optical simulations based on a dipole model [10, 46, 47]. Therein Θ is defined as the second moment of the angular distribution function of the transition dipole moment (TDM) vectors of the emissive species:

$$\Theta = < \cos^2 \vartheta > \tag{4}$$

where $< \ldots >$ represents the average over all molecules in the film and ϑ is their individual TDM vector's angle to the substrate normal. The order parameter takes a value of $\Theta = 0$ if the TDM vectors all lie in the substrate plane, i.e. horizontal, whereas $\Theta = 1$ indicates that all TDM vectors stand upright on the substrate, i.e. vertical, and for random TDM vector orientation distribution in the film, one gets $\Theta = 0.33$. In terms of light extraction from OLEDs, a Θ value as small as possible is preferred, which is equivalent to predominantly horizontal emitter TDM orientation [8, 10, 37].

Figure 3 shows an exemplary ADPL result for the yellow Ir emitter in the cohost system with the best horizontal orientation among the studied 25 G-H systems. Part (a) and (b) of the figure show the raw data acquired with ADPL for p- and s-polarization of the detector with respect to the observation plane, whereas part (c) shows the extracted emission spectrum and the orientation order parameter Θ.

In this context, we would like to point out some special features of our analysis. First, our analysis does not only use a single wavelength – often only the emission peak wavelength is taken in literature – but the full emission range extending over more than 250 nm. Thus, we actually obtain a wavelength dependent orientation parameter $\Theta(\lambda)$ over a broad wavelength range, which is then weighted with the emission intensity at each wavelength and averaged over the whole detected spectral range, similar to Ref. [46]. In this way, we obtain a spectrally weighted average Θ value that is less prone to measurement noise and fluctuations (see Figure 3c). Typically, $\Theta(\lambda)$ does not vary much over the spectral emission range, and its average value is very close to

21951071, 2026, 8, Downloaded from https://advanced.onlinelibrary.wiley.com/doi/10.1002/adom.202600902 by Open Access University of Augsburg - Universitätsbibliothek Augsburg , Wiley Online Library on [23/02/2026]. See the Terms and Conditions (https://onlinelibrary.wiley.com/terms-and-conditions) on Wiley Online Library for rules of use; OA articles are governed by the applicable Creative Commons License

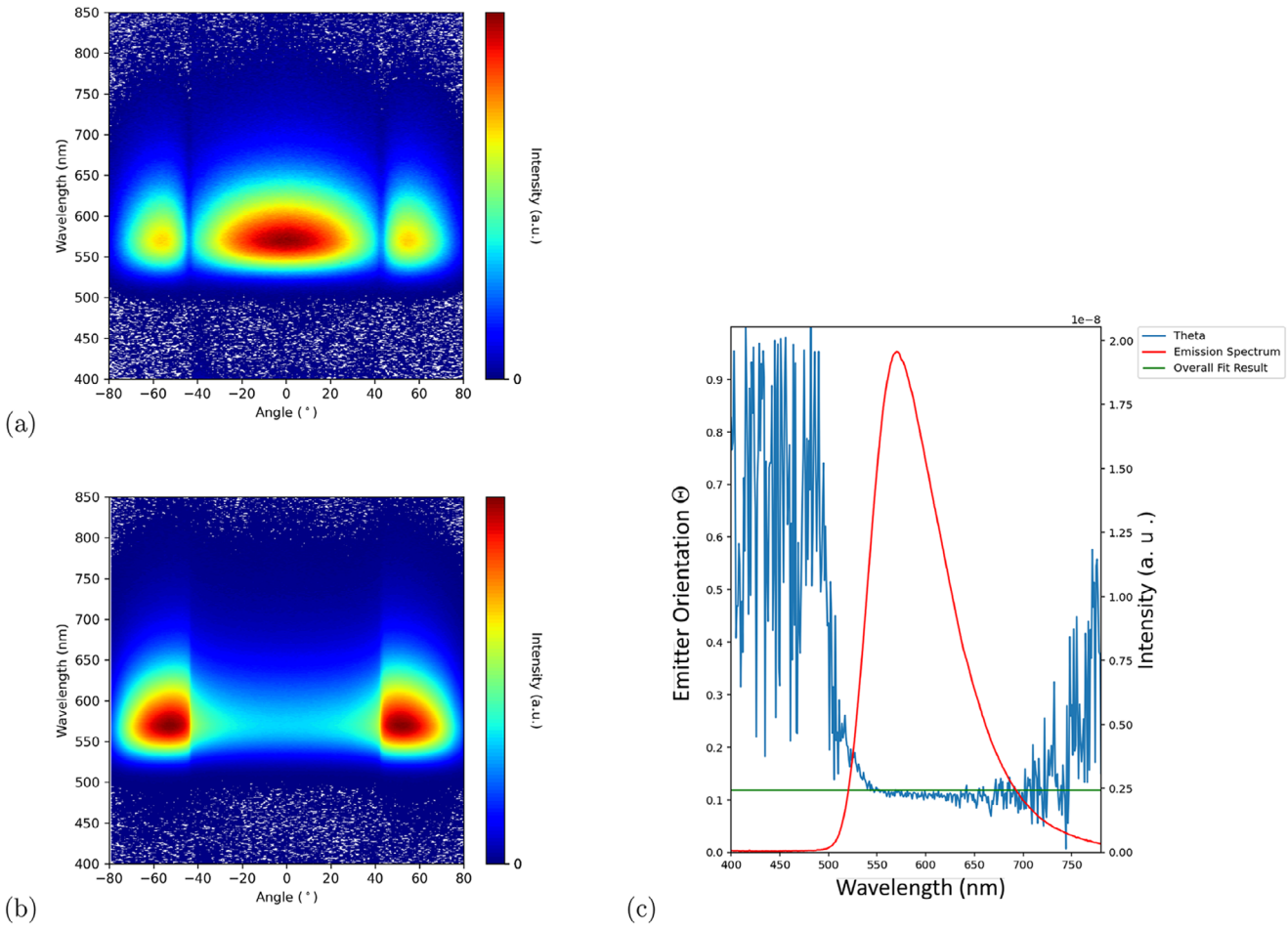

FIGURE 3 | (a) Measured p-pol. and (b) s-pol. angle dependent photoluminescence spectra for the best horizontally oriented G-H system (sample 25). (c) Shows the extracted "intrinsic" emission spectrum (red line) as well as the wavelength dependent orientation parameter $\Theta(\lambda)$ (blue line). The weighted average orientation parameter Θ (green line) is 0.119 in this case.

$\Theta(\lambda_{max})$ at the emission peak wavelength, but deviations of the order of 0.01–0.02 are observed in some cases.

Second, we do not even use an emission spectrum as an input parameter for the wave-optical analysis, but extract an "intrinsic" spectrum of the emissive dipoles as if they were embedded in an infinite medium having the refractive index of the host material. This is the spectrum shown in Figure 3c. The reason is that any experimentally measured emission spectrum, which is used as input, will be affected by thin-film interference effects and does therefore not correspond to the "intrinsic" spectrum needed for the emissive dipole model [48].

Third, we also want to highlight that we do not only analyze the p-polarized part of the ADPL measurement (as it is typically done in literature; see e.g. [11, 36]), but also its s-polarized contribution. This may seem redundant because all the information on dipole orientation is exclusively contained in the former, while the latter only yields the film thickness, which is around 30 nm in all samples. Nevertheless, the analysis of both, s- and p-pol. parts, is an important consistency check [46] and indicates whether or not the birefringence of the host materials have been properly taken into account.

As an example, Figure 4 shows both the s- and p-polarized signals at the peak emission wavelength for the G-H system with the best horizontal orientation ($\Theta = 0.119$; sample 25 with $\Delta n = -0.181$) and the worst one ($\Theta = 0.195$; sample 1 with $\Delta n = 0.031$). The agreement between measured data (red and green dots) and the corresponding fits (red and green lines) is excellent, yielding an overall error in the orientation parameter as low as 0.001 in some cases, but never larger than 0.015 in all of the studied 25 samples (see Supporting Information). However, the fact that there is a difference of both G-H systems not only in the p-polarized contribution – because of different emitter orientation – but also in their s-polarized component, is a clear indication for different refractive indices of the two systems, specifically their birefringence. This is demonstrated by the simulated ADPL curves (black lines) in Figure 4 for the case of two different emitter orientations ($\Theta = 0$ dotted lines, $\Theta = 0.33$ dashed lines) in an otherwise identical host with non-birefringent optical constants. In that case, the s-pol. curves are identical – regardless of emitter orientation – as expected. This in turn means that the obvious difference of the measured s-pol. curves between the two samples is a fingerprint of different birefringence of the corresponding host materials. If this is neglected, e.g. by assuming isotropic optical constants, an error of about 0.02 in the extracted

21951071, 2026, 8, Downloaded from https://advanced.onlinelibrary.wiley.com/doi/10.1002/adom.202600902 by Open Access University of Augsburg - Universitätsbibliothek Augsburg , Wiley Online Library on [23/02/2026]. See the Terms and Conditions (https://onlinelibrary.wiley.com/terms-and-conditions) on Wiley Online Library for rules of use; OA articles are governed by the applicable Creative Commons License

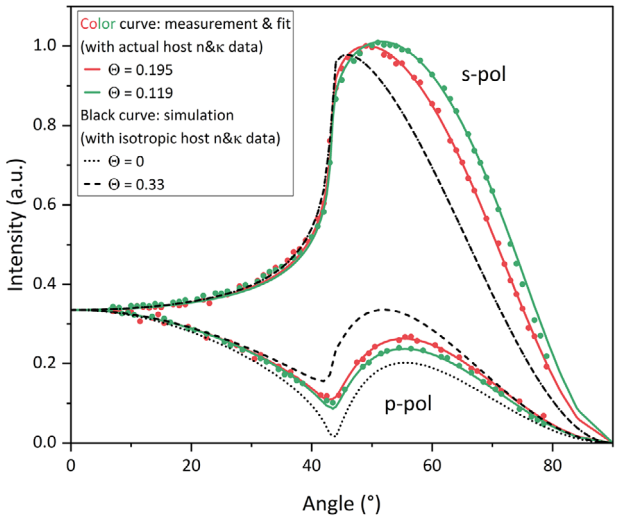

FIGURE 4 | Exemplary ADPL measurement and orientation fits (both p- and s-pol) at the peak emission wavelength for the two G-H systems with the lowest (green line, sample 25) and highest (red line, sample 1) Θ values, respectively, using the measured optical constants of the respective cohost systems. Also shown are simulations for the case of random and perfectly horizontal emitter orientation in an isotropic host.

orientation parameter is obtained, which is clearly larger than the accuracy of our analysis.

We also want to comment on the thickness of the emissive layer and the width of the emission zone in the optical simulation of ADPL measurements. In our analysis, we assumed a sharply localized ("δ-shaped") dipole emission in the center of the 30 nm thick organic layer sitting on top of a fused silica substrate. In a recent work, Jin et al. have shown that a distributed emission zone is only required, if the layer thickness exceeds 50 nm or if the sample contains additional organic layers [49]. Therefore, we kept our layer stack very simple and used a thickness well below this limit to avoid the additional effort of taking a distributed emission zone into account. Anyhow, as shown by their analysis, the error on the orientation parameter Θ is less than 0.02, if the layer thickness stays below the critical value.

Now turning to the variation of emitter TDM orientation within the investigated G-H systems. Figure 5 shows plots of the extracted Θ values vs. different properties of the cohost materials, like (a) their birefringence Δn and (b) their S parameter. In part (c) of the graph, we plot the S parameter of the cohosts vs. their Δn values. Finally, (d) shows a plot of emitter orientation Θ vs. the effective glass transition temperature $T_{g,\mathrm{eff}}$ of the cohosts.

The first two representations show a clear tendency between emitter orientation and the host properties. However, the (linear) correlation is best between Θ of the emitter and the S parameter of the cohost, as displayed in Figure 5b. This shows that cohost molecules with preferential horizontal orientation (negative S values) promote codeposited emitter molecules to orient preferentially horizontal as well. This can be understood as a consequence of van der Waals forces between emitter molecules landing on the surface of the growing film and host molecules being already there. Neglecting permanent dipole moments, the van der Waals (i.e. dispersion) forces between two neutral molecules are proportional to the product of their polarizabilities. However, since the polarizability of a molecule is a tensor, these forces are highly anisotropic and thus depend strongly on the relative orientation between the two partners. One can therefore envision that alignment of one species, e.g. with the largest component of the polarizability tensor in the film plane, drives the alignment of the other species so that the interaction is maximized. This argument is qualitatively valid for a correlation of emitter orientation Θ with both, the birefringence Δn as well as the S parameter of the cohost. Apparently, the latter one is more significant in our data, similar to the results by Huh et al. [33].

One subtle but important difference between both parameters (Δn and S) is that S is a real order parameter, i.e. it is per definition normalized (see Equation 1) between the two limiting values of $S = -0.5$ (horizontal) and $S = 1$ (vertical), while Δn is not. This means that increasing Δn of the cohost – either in positive or negative direction – does not necessarily mean that the host molecules have better alignment; it could just mean that the refractive index "contrast" on individual molecules is larger. For this reason, we have normalized the birefringence of the studied cohost materials by dividing Δn by the so-called effective isotropic refractive index:

$$n_{\mathrm{iso}} := \sqrt{(2n_o^2 + n_e^2)/3} \tag{5}$$

However, as shown in Figure S9, this did not change the observed trend and the quality of the correlation is basically unchanged. This also holds, if instead of the effective S parameter of the cohost matrices, only the dominant S_e or S_h parameter is taken (Figure S10). This in turn confirms that the analysis of emitter orientation vs. the cohosts' properties is robust with respect to the details of obtaining their optical anisotropy.

Interestingly, it seems that there are two groups of cohost materials with different correlation between their S and Δn values, as shown in part (c) of Figure 5. Nevertheless, without detailed microscopic modeling, it is hard to judge whether the apparent saturation of emitter orientation for increasingly larger negative birefringence of the cohost (see Figure 5a) is significant or not; at least, it is not that pronounced in the plot of emitter orientation vs. S of the cohost (see Figure 5b). We want to note that the apparent "outliers" (samples 13, 17 and 18) are somewhat special, because they combine an extremely negative birefringent, i.e. lying, e-type host component with an almost isotropic h-type one (see Supporting Information for details). Thus, one may additionally ask how good the miscibility of both of them is, and whether the Ir emitter complex is well dispersed in both compounds or prefers one above the other. However, this is beyond the scope of our study.

Another molecular orientation mechanism that is often discussed, is based on the surface equilibration model [50]. While originally put forward for single-component films prepared by physical vapor deposition, there is growing evidence that it also applies to multi-components systems, like the ones studied here [51, 52]. In essence, it says that the time span for diffusion and reorientation of molecules on the surface of a film during

21951071, 2026, 8, Downloaded from https://advanced.onlinelibrary.wiley.com/doi/10.1002/adom.202600902 by Open Access University of Augsburg - Universitätsbibliothek Augsburg , Wiley Online Library on [23/02/2026]. See the Terms and Conditions (https://onlinelibrary.wiley.com/terms-and-conditions) on Wiley Online Library for rules of use; OA articles are governed by the applicable Creative Commons License

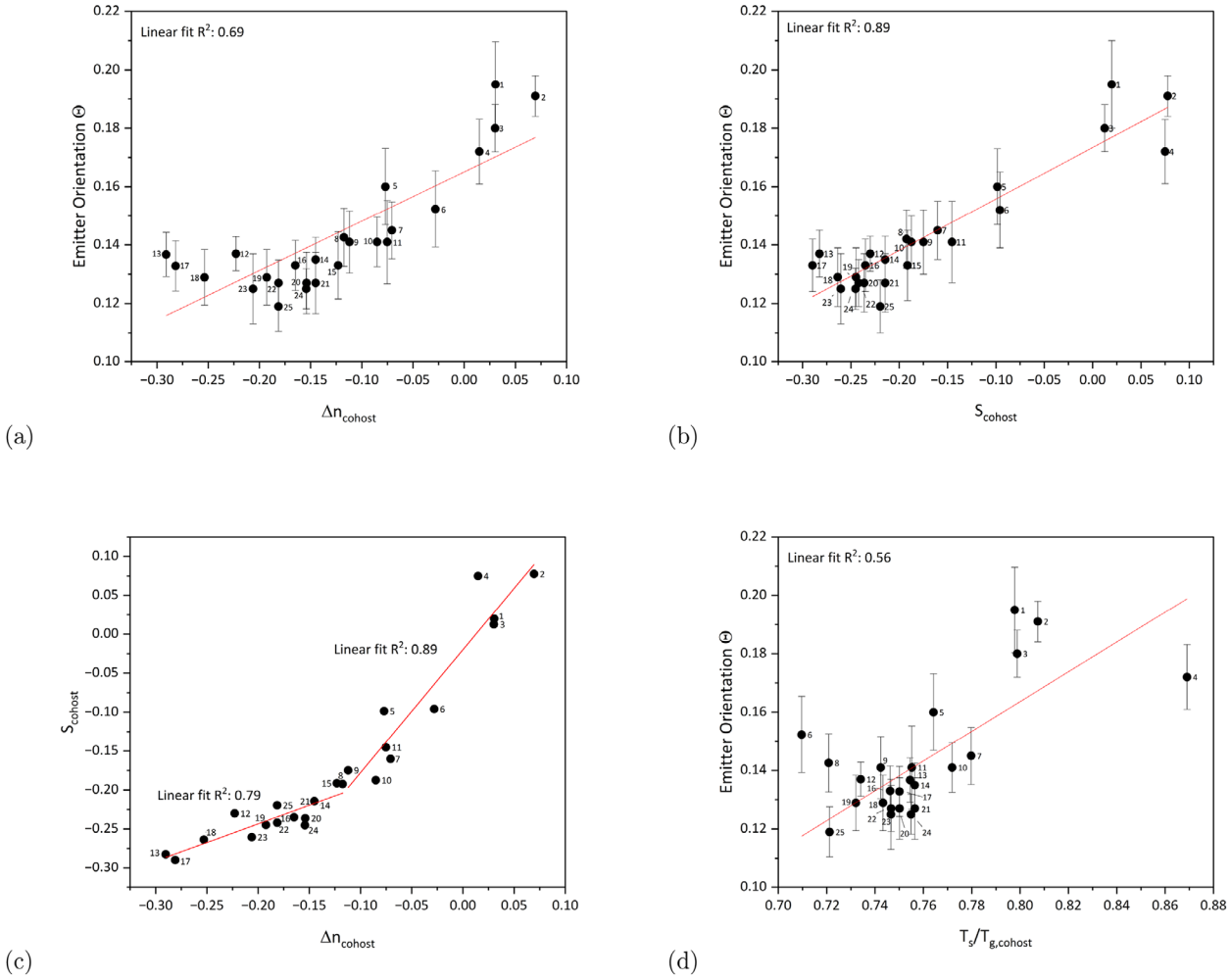

FIGURE 5 | Correlation of emitter orientation with different properties of the 25 different cohost materials: (a) Emitter orientation vs. Δn of cohosts, (b) emitter orientation vs. S parameter of cohosts, (c) S parameter of cohosts vs. their Δn, and (d) emitter orientation vs. $T_S/T_{g,\mathrm{eff}}$ of cohosts, where the used substrate temperature T_S was room temperature in all samples.

physical vapor deposition, before they are covered by a layer of newly deposited molecules, determines their final orientation in the bulk of the film. If deposition is fast, i.e. at high rate, or molecular motion is slowed down by cooling the substrate, horizontal orientation is more likely. Besides deposition rate, the most important parameter is the substrate temperature T_S in relation to the glass transition temperature T_g of the material that is grown as a film. In the case of a G-H system, it has been shown that instead of changing T_S, the use of hosts with different T_g's is equally powerful to control emitter orientation [14, 15, 53].

Thus, in Figure 5d we plot the extracted emitter orientation vs. the ratio of $T_S/T_{g,\mathrm{eff}}$ of the used 25 cohost systems, with T_S being room temperature in all samples. In this case, we obtain the worst correlation of all the shown graphs. This does not mean that there is no correlation between Θ of the emitter and the cohost's $T_{g,\mathrm{eff}}$, especially since the Δn and S values of the host materials are in itself expected to correlate with their effective T_g's, but the scattering of the data is relatively large. At this point, we want to note that the used T_g values of the neat host materials were either directly measured or obtained from calculations [54]. Nevertheless, the calculated $T_{g,\mathrm{eff}}$ values may have a substantially larger error bar than Δn and S of the cohost systems.

To summarize, we find a clear correlation between the degree of horizontal alignment of the studied Ir emitter complex and the optical anisotropy of the cohost materials. Specifically, cohosts with negative birefringence (or negative S parameter), i.e. preferentially lying molecules, promote better horizontal alignment of the emitter as well. This is understandable because the studied emitter complex does not have an ancillary ligand or other chemical anisotropies that would cause the electrostatic surface potential to vary strongly and would promote specific alignment. Thus, in the absence of such "chemical driving forces", the alignment of the emitter molecule is driven by anisotropic London dispersion interactions with the host, which can be modified by changing the direction and magnitude of the host's optical birefringence in thin films (or its S parameter).

3.2 | Application to Light Outcoupling in OLEDs

In our previous work on a series of green emitting Ir complexes, we observed a strong boost in OLED efficiency by tuning their emissive TDM orientation [37]. Specifically, we observed an increase from about 20% to 30% EQE, i.e. relatively speaking by 50%, if their orientation parameter Θ decreases from an

21951071, 2026, 8, Downloaded from https://advanced.onlinelibrary.wiley.com/doi/10.1002/adom.202600902 by Open Access University of Augsburg - Universitätsbibliothek Augsburg , Wiley Online Library on [23/02/2026]. See the Terms and Conditions (https://onlinelibrary.wiley.com/terms-and-conditions) on Wiley Online Library for rules of use; OA articles are governed by the applicable Creative Commons License

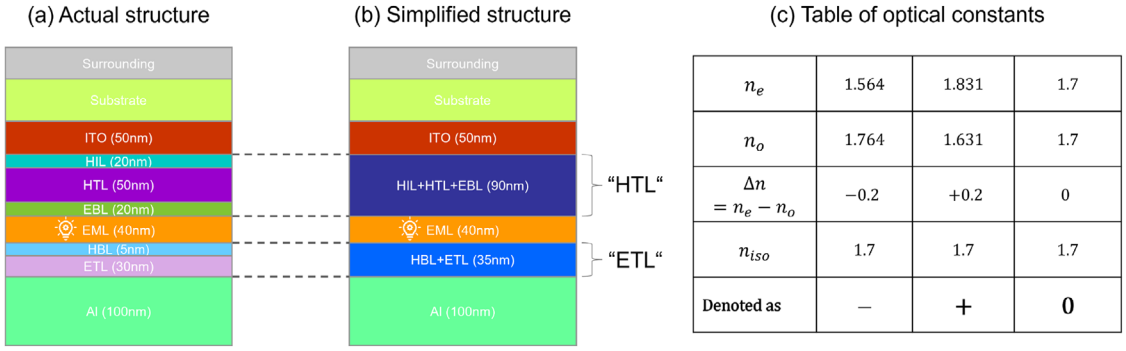

FIGURE 6 | Used OLED stack for measuring EQE in devices: (a) Actual layer stack with different functionalities on both the hole and electron transport side; (b) simplified layer stack with only one "effective" hole transport layer and one "effective" electron transport layer of corresponding thicknesses. (c) The table on the right shows the used refractive indices for birefringent layers with the same effective isotropic refractive index of 1.7 in all cases. (Acronyms denote the following: ITO – indium-tin oxide, HIL – hole injection layer, HTL – hole transport layer, EBL – electron blocking layer, EML – emission layer, HBL – hole blocking layer, ETL – electron transport layer, Al – aluminum. The substrate is glass with a refractive index of 1.5 and a thickness of 1 mm; the surrounding medium, into which light is extracted, is semi-infinite air with $n = 1$).

isotropic value around 0.33 to 0.14. Thus, we were expecting a corresponding enhancement of OLED efficiency by an absolute value of roughly 5%, if we change the orientation of the emitter from 0.2 to 0.1. However, one has to keep in mind, that in our former work, the host material was identical in all the studied OLEDs, while its properties are now changing as we change the composition of the cohost mixtures.

Importantly, for all investigated cohost pairs, a systematic variation of the e- to h-type cohost composition was performed in an OLED test structure to identify the optimum ratio of both constituents in terms of device efficiency. Exemplary device characteristics for the two cohost pairs from Figure 2 that were used in devices 4 and 21 are given in Section S6. In this case we find an optimal h/e-cohost ratio ($c_h/(c_e + c_h)$) of 34% in device 4- (i.e. electron dominated) and 67% (i.e. hole dominated) in device 21. OLEDs with non-optimum cohost composition may show significantly reduced device efficiency due to substantial deviations in the location of the recombination zone within the emission layer, which may increase the likelihood of quenching events within the EML or at its interfaces and/or drastically impact the light outcoupling, as will be shown by simulation below. While only optimized cohost compositions can therefore serve to study the impact of emitter orientation on device efficiency, also non-optimum compositions were included in the above-described orientation study in order to maximize the attainable range of the optical anisotropy. These considerations resulted in a subset of 12 G-H systems that are used to study possible correlations between the measured emitter orientation and the external quantum efficiency of the corresponding OLEDs. Their EQEs are specified in Table S1. These EQE values were extracted at an application relevant current density of 10 mA/cm^2 in all devices, which corresponds to luminance values of typically about 10 000 cd/m^2. Note that the maximum EQE, achieved at lower current density and luminance, was typically 2–3% higher in many of the devices (see Figures S11 and S12).

The used OLED layer stack is shown in Figure 6a. It is a bottom-emitter structure with a 40 nm thick emission layer (EML) sandwiched between a total of 90 nm thick layers on the hole transport side (consisting of hole injection and transport as well as electron blocking layers) and a 35 nm layer on the electron transport side (consisting of hole blocking and electron transport layers). These transport layers were kept identical in all OLEDs with the different emissive G-H systems. Figure 7 shows the measured EQEs plotted vs. the emitter orientation of the respective G-H combinations. Surprisingly, despite a reduction in emitter orientation from $\Theta = 0.195$ (sample 1) to 0.119 (sample 25) the improvement in EQE is only moderate, i.e. in the range 1–2% in the best cases.

For further insights into the potential of EQE enhancement by the more horizontal emitter orientation in the studied anisotropic G-H systems, we performed wave-optical simulations based on an emissive dipole model [5] using the commercial OLED simulation software SETFOS by Fluxim. To this end, we simplified the actual OLED stack further, as indicated in Figure 6b, using a total of 90 nm hole transport layers ("HTL") and 35 nm electron transport layers ("ETL") with constant, i.e. wavelength-independent optical parameters ($n = 1.7$ and $\kappa = 0$). To start with, we used an optically isotropic host (i.e. $\Delta n = 0$) and varied the emitter TDM orientation parameter $\Theta = 0.2 \rightarrow 0.1$. For the emission zone (EMZ), we used three different scenarios: a) an exponential profile located at the HTL side of the EML ($x = 0$) with a decay length of 10 nm, b) a Gaussian profile located in the center of the EML ($x = 0.5$) with a double-sided decay length of 10 nm, and c) an exponential profile located at the ETL side of the EML ($x = 1$) with a decay length of 10 nm. The simulated curves are shown as dashed lines in Figure 7, and the obtained EQEs for the limiting orientations ($\Theta = 0.1$ and 0.2) are given in Table 1 (Cases 1a–c). We find that the experimental data are all within the range described by these three scenarios. In detail, the devices with electron-dominated cohosts (1,4,5) seem to be better described by scenario a) with the EMZ closer to the HTL, while the other devices (with mostly hole-dominated cohosts) seem to have their EMZ in the middle of the EML or closer to the ETL side – see also the simulations for a variation of the EMZ location in Figure S13.

In all three scenarios, an absolute increase of the EQE by 5–6% is predicted between the limiting values of the orientation parameter (see Table 1). As this would amount to a relative increase

21951071, 2026, 8, Downloaded from https://advanced.onlinelibrary.wiley.com/doi/10.1002/adom.202600902 by Open Access University of Augsburg - Universitätsbibliothek Augsburg , Wiley Online Library on [23/02/2026]. See the Terms and Conditions (https://onlinelibrary.wiley.com/terms-and-conditions) on Wiley Online Library for rules of use; OA articles are governed by the applicable Creative Commons License

TABLE 1 | Simulated light outcoupling of the OLED stack with simplified optical data for the two limiting orientation values of $\Theta = 0.1$ and 0.2. "+", "−" and "0" indicate positive, negative and no birefringence in the respective layers. For the emission zone we either take exponential profiles with a decay length of 10 nm, where $x = 0$ refers to the HTL side and $x = 1$ to the ETL side of the EML, or a Gaussian profile (centered at $x = 0.5$ with 10 nm decay length to both sides).

Case	HTL	EML	ETL	Light outcoupling (%)		EMZ location and width	Comment
				$\Theta = 0.1$	$\Theta = 0.2$		
1a	0	0	0	33.7	28.9	Exp ($x = 0$/10nm)	isotropic host
1b	0	0	0	32.5	27.0	Gauss ($x = 0.5$/10nm)	isotropic host
1c	0	0	0	29.6	23.6	Exp ($x = 1$/10nm)	isotropic host
2a	0	+	0	—	29.3	Exp ($x = 0$/10nm)	standing host
2b	0	+	0	—	27.6	Gauss ($x = 0.5$/10nm)	standing host
2c	0	+	0	—	24.4	Exp ($x = 1$/10nm)	standing host
3a	0	—	0	33.4	—	Exp ($x = 0$/10nm)	lying host
3b	0	—	0	32.0	—	Gauss ($x = 0.5$/10nm)	lying host
3c	0	—	0	28.7	—	Exp ($x = 1$/10nm)	lying host
4	+	+	—	37.5	31.7	Gauss ($x = 0.5$/10nm)	best case
5	—	—	+	28.1	22.9	Gauss ($x = 0.5$/10nm)	worst case

of about 17–20%, the potential impact of the emitter orientation on the OLED's EQE is very large. But clearly, such a strong EQE enhancement is not observed in the experimental data. Apart from the already discussed shift of the EMZ location with varied cohost mixing ratio, another important factor has not been considered so far: the variation of the (co)hosts' birefringence We have to remember that the (co)host material in the EML is not staying isotropic, as we move from "bad" emitter orientation ($\Theta = 0.2$) to "good" orientation ($\Theta = 0.1$). Actually, the improved more horizontal emitter orientation goes along with a change in birefringence of the host materials as well. In fact, the key point of our approach is to induce more horizontal emitter orientation by host materials that are aligning more horizontally themselves, i.e. they become more negatively birefringent as discussed in the context of Figure 5. However, this change of Δn in the OLED's EML can have an effect on light outcoupling as well.

To verify this effect, we performed another series of optical simulations including now also the change of the optical constants, i.e. the birefringence, of the EML. Specifically, we assumed a (co)host material with positive birefringence $\Delta n = +0.2$ at $\Theta = 0.2$ and negative birefringence $\Delta n = -0.2$ at $\Theta = 0.1$ and simulated the light outcoupling for all three scenarios of the EMZ location; see the stars in Figure 7 as well as the numbers in Table 1. Now it becomes apparent that the host's positive birefringence (at $\Theta = 0.2$, Cases 2a–c) improves light outcoupling by about 0.5–1%, while the negative Δn (at $\Theta = 0.1$, Cases 3a-c) decreases it by the same amount, regardless of the exact location of the EMZ. This is visualized by the colored arrows in Figure 7. The reason is that in terms of light outcoupling, a host with positive birefringence is preferred, because under these conditions one has less coupling of the emissive dipoles to the substrate and other lossy modes in the OLED. Overall, we get a slightly weaker dependence of light outcoupling on emitter orientation, if we connect the two limiting cases (i.e. the stars) by a full line, as shown for a Gaussian EMZ in the center of the EML (red line in Figure 7).

On the other hand, it is understandable that our cohost systems with considerable variations of e- and h-type host composition, having different carrier mobility each as well as different energy levels, exhibit variations of their emission zone locations that have an effect on their light outcoupling factor comparable to what is expected based on a change of the emitter TDM orientation alone. In addition, some of the materials used in the OLED stack (including the emitter itself) are dipolar molecules and can show spontaneous orientation polarization, i.e. alignment of their electrical dipole vectors [55, 56]. This induces an inhomogeneous internal electrical field distribution that can lead to charge accumulation at interfaces and other effects, like exciton-polaron quenching [57–59], which affect the efficiency of OLEDs beyond their purely optical design. This taken all together, can explain the relatively large scatter of the EQE data observed in Figure 7. However, even with these uncertainties, one can expect a substantial improvement in light outcoupling between an emitter orientation of $\Theta = 0.2$ in a host with positive $\Delta n = 0.2$, and $\Theta = 0.1$ in a host with negative $\Delta n = -0.2$ of about 4% in absolute numbers, i.e. relatively speaking by about 13%. And, experimentally we see this trend being followed by the data as well, though perhaps with a slightly lower EQE enhancement of about 1.5% only in absolute numbers.

For a more general view of the role of optical anisotropy in OLEDs, we extended the device simulations and varied the birefringence in all three compartments of the OLED stack, i.e. HTL, EML and ETL, for this yellow emitter. For simplification, we have again used wavelength independent refractive indices in all layers (setting $\kappa = 0$) and considered three cases with $\Delta n = 0$ and ± 0.2 in each of the layers, i.e. 27 combinations in total. Thereby, we made sure that the average "isotropic" refractive index, as defined in Equation 5, is 1.7 in all cases. The corresponding values of n_o and n_e for the different cases are given in the table on the right side of Figure 6. As listed in Table 1 (Cases 4 and 5), the best result is obtained for a combination of birefringence in the different layers as (+|+|−) in HTL|EML|ETL with an outcoupling value

21951071, 2026, 8, Downloaded from https://advanced.onlinelibrary.wiley.com/doi/10.1002/adom.202600902 by Open Access University of Augsburg - Universitätsbibliothek Augsburg , Wiley Online Library on [23/02/2026]. See the Terms and Conditions (https://onlinelibrary.wiley.com/terms-and-conditions) on Wiley Online Library for rules of use; OA articles are governed by the applicable Creative Commons License

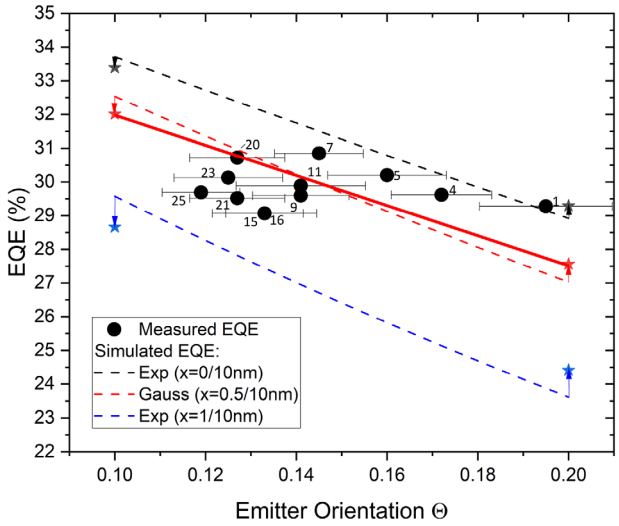

FIGURE 7 | Measured EQEs of 12 OLEDs with optimized cohost compositions and emitter orientation parameters as determined above. The dashed lines show the simulated EQE vs. emitter orientation for the simplified OLED stack in Figure 6 with isotropic refractive indices ($n = 1.7$) in all layers, assuming different locations and shapes of the EMZ within the EML. Additionally, we show simulated EQE values (stars) for the same three different locations of the EMZ for an orientation $\Theta = 0.1$ in a lying host ($\Delta n = -0.2$) and $\Theta = 0.2$ in a standing host ($\Delta n = +0.2$). The full red line is a linear connection between these data points for a centered Gaussian EMZ.

of 37.5% (for $\Theta = 0.1$), whereas the worst is (−| − |+) with only 28.1% outcoupling for the same emitter orientation. This result is in agreement with simulation results by Callens et al. [60], as far as the role of birefringence in HTL and ETL are concerned. However, we now also consider the important role of Δn in the EML itself, which was not done in previous work. Importantly, we find the unexpected result that negative birefringence in the EML compromises light outcoupling, although it promotes horizontal emitter orientation.

Overall, the potential of tuning EQE in an OLED by birefringence in the individual layers of the stack is large. As indicated by the last two lines in Table 1, a change in the EQE by almost 9% in absolute numbers is possible between the best case of (+| + |−) in (HTL|EML|ETL) as compared to the worst case scenario of (−| − |+) at a given emitter orientation. And if the emitter orientation is changing as well, the variation can be as large as 14% in absolute EQE. Thus, birefringence in all layers of an OLED – including the emissive guest-host system – is of paramount importance for maximizing their efficiency.

4 | Conclusion

We have demonstrated that the emitting dipole orientation of a low-symmetry Ir complex is correlated with the optical anisotropy of the (co)host material used for the emissive layer in OLEDs. Since the chosen Ir complex does not have an ancillary ligand or specific functional groups that would lead to a pronounced asymmetry in its electrostatic surface potential, the main driving forces for horizontal alignment during physical vapor deposition are London dispersion-type van der Waals interactions. This means that the molecular polarizability tensor of the emitter complex will try to align in line with the direction of birefringence of the host material. Thus, emitter orientation can be tuned by varying the optical anisotropy of the (co)host material by mixing e- and h-type constituents with different degree of birefringence.

However, in terms of OLED efficiency, the optical anisotropy of the host material has two effects: It improves emitter orientation toward more horizontal TDM alignment, yielding more directly emitted light, but it also enhances lossy optical modes in an OLED so that light outcoupling is compromised, if Δn of the host becomes too negative. Thus, achieving optimum light outcoupling by tuning the optical anisotropy of the host material requires to find a sweet spot of Δn for improving emitter orientation but not degrading light outcoupling too much.

Furthermore, the cohost composition in terms of e- and h-type components is critical as well, because it influences the position (and width) of the recombination zone within the emissive layer, which in turn has effects on the light outcoupling factor of the OLED that can be comparable to the influence of emitter orientation itself. Nevertheless, as we have demonstrated experimentally, OLEDs with already good performance can be optimized further by promoting more horizontal emissive dipole orientation through the use of a preferentially lying (co)host material.

5 | Experimental Section

5.1 | Density Functional Theory (DFT)

DFT calculations were performed on the Ir emitter complex using the Schrödinger Materials Science Suite to obtain the polarizability tensor and the electrostatic surface potential (ESP) map of the optimized structure. Using the Jaguar optimization function in the software, we calculated the polarizability tensor using the B3PW91 functional and the 6–31G* basis set (specifically, the LANL2DZ basis set was applied for the Ir atom). The ESP of the emitter was mapped using Poisson–Boltzmann ESP tool on an optimized structure.

5.2 | Variable Angle Spectroscopic Ellipsometry (VASE)

The optical constants of the used cohost system were determined by VASE using a J.A. Woollam RC2 ellipsometer. To this end, organic films were evaporated on Si wafers with a thin native oxide layer on their surface. The measurements of the two ellipsometric parameters (Ψ, Δ) were conducted at variable angles between 40° and 70° with respect to the substrate normal, with a step size of 5° in the wavelength range 250–1000 nm. These (Ψ, Δ) spectra were subsequently fitted with a suitable oscillator model (typically, a series of Lorentz oscillators was used to account for the observed resonances) and film thickness as well as refractive index $n(\lambda)$ and extinction coefficient $\kappa(\lambda)$ were extracted.

21951071, 2026, 8, Downloaded from https://advanced.onlinelibrary.wiley.com/doi/10.1002/adom.202600902 by Open Access University of Augsburg - Universitatsbibliothek Augsburg , Wiley Online Library on [23/02/2026]. See the Terms and Conditions (https://onlinelibrary.wiley.com/terms-and-conditions) on Wiley Online Library for rules of use; OA articles are governed by the applicable Creative Commons License

5.3 | Angular-Dependent Photoluminescence (ADPL)

Emitter orientation was obtained from ADPL measurements on a PHELOS instrument from Fluxim AG. The emissive G-H system was co-evaporated on a fused silica substrate and mounted by an index-matching fluid on a rotatable cylindrical lens. The sample was excited by a 365 nm UV LED from the top and the PL emission was monitored through the cylindrical lens. To this end, the lens was rotated in front of a polarizer and an optical fiber that was coupled to a CCD spectrometer with a detection range between 400 and 850 nm. The PL intensity was measured for both s- and p-polarization at variable angles, ranging from −90° to +90°, with a step size of 1°.

The obtained PL radiation pattern of the sample was subsequently analyzed by a home-built wave-optical simulation software based on a dipole model [10]. The only required input parameters were the optical constants n, κ in the corresponding wavelength range, whereas the "intrinsic" emission spectrum of the G-H system was extracted from simulation. First, the s-pol. spectrum was fitted to determine the film thickness. Once the film thickness was known, the p-pol. spectrum can be fitted to obtain the orientation parameter Θ.

5.4 | OLED Fabrication

OLED devices were fabricated by successive deposition of organic layers by thermal evaporation in a commercially available high-vacuum chamber with a base pressure below 10^{-7} mbar. Glass plaques coated with a structured ITO anode of thickness 50 nm served as substrate after a successive pre-treatment with an oxygen plasma and an argon plasma. The OLEDs have the following layer structure: substrate, hole injection layer (HIL), hole transport layer (HTL), electron blocking layer (EBL), emission layer (EML), hole blocking layer (HBL), electron transport layer (ETL), electron injection layer (EIL) and finally a cathode. The cathode was formed by thermal evaporation of a layer of aluminium with a total thickness of 100 nm. Layer deposition rates were controlled using a quartz crystal microbalance after layer thickness calibration by optical ellipsometry. The employed materials in HIL, HTL, EBL and in HBL, ETL were state-of-the-art, industry-standard hole and electron transport materials, respectively.

5.5 | Optical Simulation of OLEDs

Wave-optical simulations of light outcoupling from OLEDs were performed with the software SETFOS from Fluxim AG. It is based on an emissive dipole model similar to Ref. [10]. The necessary input was the OLED layer stack including all layer thicknesses as well as their optical constants (n, κ) and the orientation and location of the emitter; its quantum efficiency was assumed to be unity. As an output, the contribution of power dissipation in different optical modes, including direct emission, substrate modes, wave-guided modes, surface plasmons and re-absorption, was calculated. Assuming unity internal quantum efficiency, the calculated out-coupling into air directly corresponds to the EQE of the device.

Acknowledgements

This work was funded by Deutsche Forschungsgemeinschaft (DFG, German Research Foundation) through a knowledge transfer project between Universität Augsburg and Merck KGaA, Darmstadt (project no. 512372385) and an instrumentation grant for VASE (project no. 530008779).

Open access funding enabled and organized by Projekt DEAL.

Conflicts of Interest

The authors declare no conflicts of interest.

Data Availability Statement

The data that support the findings of this study are available from the corresponding author upon reasonable request.

References

1. S. Reineke, "Complementary LED Technologies," *Nature Materials* 14, no. 5 (2015): 459–462.

2. S. R. Forrest, "Waiting for Act 2: What Lies Beyond Organic Light-Emitting Diode (OLED) Displays for Organic Electronics?," *Nanophotonics* 10, no. 1 (2021): 31–40.

3. G. Hong, X. Gan, C. Leonhardt, et al., "A Brief History of OLEDs–Emitter Development and Industry Milestones," *Advanced Materials* 33, no. 9 (2021): 2005630.

4. C. Adachi, M. A. Baldo, M. E. Thompson, and S. R. Forrest, "Nearly 100% Internal Phosphorescence Efficiency in an Organic Light-Emitting Device," *Journal of Applied Physics* 90, no. 10 (2001): 5048–5051.

5. W. Brütting, J. Frischeisen, T. D. Schmidt, B. J. Scholz, and C. Mayr, "Device Efficiency of Organic Light-Emitting Diodes: Progress by Improved Light Outcoupling," *Physica Status Solidi (A)* 210, no. 1 (2013): 44–65.

6. J. Frischeisen, D. Yokoyama, A. Endo, C. Adachi, and W. Brütting, "Increased Light Outcoupling Efficiency in Dye-Doped Small Molecule Organic Light-Emitting Diodes with Horizontally Oriented Emitters," *Organic Electronics* 12, no. 5 (2011): 809–817.

7. M. Flämmich, J. Frischeisen, D. S. Setz, D. Michaelis, B. C. Krummacher, T. D. Schmidt, W. Brütting, and N. Danz, "Oriented Phosphorescent Emitters Boost OLED Efficiency," *Organic Electronics* 12, no. 10 (2011): 1663–1668.

8. S.-Y. Kim, W.-I. Jeong, C. Mayr, Y.-S. Park, K.-H. Kim, J.-H. Lee, C.-K. Moon, W. Brütting, and J.-J. Kim, "Organic Light-Emitting Diodes with 30% External Quantum Efficiency Based on a Horizontally Oriented Emitter," *Advanced Functional Materials* 23, no. 31 (2013): 3896–3900.

9. M. C. Gather and S. Reineke, "Recent Advances in Light Outcoupling from White Organic Light-Emitting Diodes," *Journal of Photonics for Energy* 5, no. 1 (2015): 057607–057607.

10. T. D. Schmidt, T. Lampe, D. Sylvinson Muthiah Ravinson, P. I. Djurovich, M. E. Thompson, and W. Brütting, "Emitter Orientation as a Key Parameter in Organic Light-Emitting Diodes," *Physical Review Applied* 8, no. 3 (2017): 681.

11. K.-H. Kim and J.-J. Kim, "Origin and Control of Orientation of Phosphorescent and TADF Dyes for High-Efficiency OLEDs," *Advanced Materials* 30, no. 42 (2018): e1705600.

12. F. Tenopala-Carmona, O. S. Lee, E. Crovini, et al., "Identification of the Key Parameters for Horizontal Transition Dipole Orientation in Fluorescent and TADF Organic Light-Emitting Diodes," *Advanced Materials* 33, no. 37 (2021): 2100677.

21951071, 2026, 8, Downloaded from https://advanced.onlinelibrary.wiley.com/doi/10.1002/adom.202600902 by Open Access University of Augsburg - Universitätsbibliothek Augsburg , Wiley Online Library on [23/02/2026]. See the Terms and Conditions (https://onlinelibrary.wiley.com/terms-and-conditions) on Wiley Online Library for rules of use; OA articles are governed by the applicable Creative Commons License

13. D. Yokoyama, "Molecular Orientation in Small-Molecule Organic Light-Emitting Diodes," *Journal of Materials Chemistry* 21, no. 48 (2011): 19187.

14. C. Mayr and W. Brütting, "Control of Molecular Dye Orientation in Organic Luminescent Films by the Glass Transition Temperature of the Host Material," *Chemistry of Materials* 27, no. 8 (2015): 2759–2762.

15. B. A. Naqvi, M. Schmid, E. Crovini, et al., "What Controls the Orientation of TADF Emitters?," *Frontiers in Chemistry* 8 (2020): 060101.

16. H. Zhao, C. E. Arneson, D. Fan, and S. R. Forrest, "Stable Blue Phosphorescent Organic LEDs That Use Polariton-Enhanced Purcell Effects," *Nature* 626, no. 7998 (2024): 300–305.

17. A. Monkman, "Why Do We Still Need a Stable Long Lifetime Deep Blue OLED Emitter?," *ACS Applied Materials & Interfaces* 14, no. 18 (2021): 20463–20467.

18. O. Sachnik, Y. Li, X. Tan, J. J. Michels, P. W. Blom, and G.-J. A. Wetzelaer, "Single-Layer Blue Organic Light-Emitting Diodes with Near-Unity Internal Quantum Efficiency," *Advanced Materials* 35, no. 26 (2023): 2300574.

19. O. Sachnik, N. Kinaret, R. Saxena, et al., "Pure-Blue Single-Layer Organic Light-Emitting Diodes Based on Trap-Free Hyperfluorescence," *Nature Materials* 24 (2025): 1742–1748.

20. P. Liehm, C. Murawski, M. Furno, B. Lüssem, K. Leo, and M. C. Gather, "Comparing the Emissive Dipole Orientation of Two Similar Phosphorescent Green Emitter Molecules in Highly Efficient Organic Light-Emitting Diodes," *Applied Physics Letters* 101, no. 25 (2012): 253304.

21. M. J. Jurow, C. Mayr, T. D. Schmidt, et al., "Understanding and Predicting the Orientation of Heteroleptic Phosphors in Organic Light-Emitting Materials," *Nature Materials* 15, no. 1 (2016): 85–91.

22. T. Lampe, T. D. Schmidt, M. J. Jurow, P. I. Djurovich, M. E. Thompson, and W. Brütting, "Dependence of Phosphorescent Emitter Orientation on Deposition Technique in Doped Organic Films," *Chemistry of Materials* 28, no. 3 (2016): 712–715.

23. A. Senes, S. C. J. Meskers, H. Greiner, et al., "Increasing the Horizontal Orientation of Transition Dipole Moments in Solution Processed Small Molecular Emitters," *Journal of Materials Chemistry C* 5, no. 26 (2017): 6555–6562.

24. K.-H. Kim, S. Lee, C.-K. Moon, et al., "Phosphorescent Dye-Based Supramolecules for High-Efficiency Organic Light-Emitting Diodes," *Nature Communications* 5 (2014): 4769.

25. K.-H. Kim, J.-Y. Ma, C.-K. Moon, et al., "Controlling Emitting Dipole Orientation with Methyl Substituents on Main Ligand of Iridium Complexes for Highly Efficient Phosphorescent Organic Light-Emitting Diodes," *Advanced Optical Materials* 3, no. 9 (2015): 1191–1196.

26. K.-H. Kim, E. S. Ahn, J.-S. Huh, Y.-H. Kim, and J.-J. Kim, "Design of Heteroleptic Ir Complexes with Horizontal Emitting Dipoles for Highly Efficient Organic Light-Emitting Diodes with an External Quantum Efficiency of 38%," *Chemistry of Materials* 28, no. 20 (2016): 7505–7510.

27. S. Kim, J.-M. Kim, J. Choi, et al., "Rational Ligand Design of Heteroleptic Iridium (III) Complexes Toward Nearly Perfect Horizontal Dipole Orientation for Highly Efficient Red-Emitting Phosphorescent Organic Light-Emitting Diodes," *Advanced Functional Materials* 33, no. 48 (2023): 2214233.

28. M. C. Jung, J. Facendola, J. Kim, et al., "Molecular Alignment of Homoleptic Iridium Phosphors in Organic Light-Emitting Diodes," *Advanced Materials* 33, no. 36 (2021): 2102882.

29. M. Schmid, K. Harms, C. Degitz, et al., "Optical and Electrical Measurements Reveal the Orientation Mechanism of Homoleptic Iridium-Carbene Complexes," *ACS Applied Materials & Interfaces* 12, no. 46 (2020): 51709–51718.

30. J. S. Kim, D. Jeong, H. J. Bae, et al., "Improved Efficiency and Stability of Blue Phosphorescent Organic Light Emitting Diodes by Enhanced Orientation of Homoleptic Cyclometalated Ir (III) Complexes," *Advanced Optical Materials* 8, no. 22 (2020): 2001103.

31. J.-M. Kim, K. Y. Hwang, S. Kim, et al., "Enhancing Horizontal Ratio of Transition Dipole Moment in Homoleptic Ir Complexes for High Outcoupling Efficiency of Organic Light-Emitting Diodes," *Advanced Science* 9, no. 31 (2022): 2203903.

32. C.-K. Moon, K.-H. Kim, J. W. Lee, and J.-J. Kim, "Influence of Host Molecules on Emitting Dipole Orientation of Phosphorescent Iridium Complexes," *Chemistry of Materials* 27, no. 8 (2015): 2767–2769.

33. J.-S. Huh, K.-H. Kim, C.-K. Moon, and J.-J. Kim, "Dependence of Pt(II)-Based Phosphorescent Emitter Orientation on Host Molecule Orientation in Doped Organic Thin Films," *Organic Electronics* 45 (2017): 279–284.

34. J.-S. Huh, K.-H. Kim, and J.-J. Kim, "Emitting Dipole Orientation and Molecular Orientation of Homoleptic Ir (III) Complexes," *Organic Electronics* 82 (2020): 105715.

35. H.-D. Lee, H. J. Jang, J. H. Baek, et al., "Preferred Orientation Evolution of Hole Transport Materials for High Emitting Dipole Orientation Ratio of the Emitting Material," *Advanced Optical Materials* 11, no. 2 (2023): 2202109.

36. H. J. Jang and J. Y. Lee, "Key Factor Managing the Horizontal Emitting Dipole Orientation of a Thermally Activated Delayed Fluorescence Emitter in a Mixed Host," *ACS Applied Materials & Interfaces* 14, no. 49 (2022): 54907–54913.

37. C. Degitz, M. Schmid, F. May, et al., "From Molecule to Device: Prediction and Validation of the Optical Orientation of Iridium Phosphors in Organic Light-Emitting Diodes," *Chemistry of Materials* 35, no. 1 (2022): 295–303.

38. P. Stoessel, A. Auch, F. May, and J. Pfister, "Metal Complexes (Patent WO2018178001A1)," Patent WO2018178001A1, 2018, https://patents.google.com/patent/WO2018178001A1.

39. P. Stoessel, A. Auch, F. May, and J. Pfister, "Metal Complexes (Patent US11569458B2)," Patent US11569458B2, 2023, https://patents.google.com/patent/US11569458B2/.

40. V. A. Markel, "Introduction to the Maxwell Garnett Approximation: Tutorial," *Journal of the Optical Society of America A* 33, no. 7 (2016): 1244–1256.

41. Y. Tsuchiya, N. Nakamura, S. Kakumachi, K. Kusuhara, C.-Y. Chan, and C. Adachi, "A Convenient Method to Estimate the Glass Transition Temperature of Small Organic Semiconductor Materials," *Chemical Communications* 58, no. 80 (2022): 11292–11295.

42. F. London, "The General Theory of Molecular Forces," *Transactions of the Faraday Society* 33 (1937): 8b–26.

43. F. M. Fowkes, "Surface Effects of Anisotropic London Dispersion Forces in N-Alkanes," *The Journal of Physical Chemistry* 84, no. 5 (1980): 510–512.

44. J. Frischeisen, D. Yokoyama, C. Adachi, and W. Brütting, "Determination of Molecular Dipole Orientation in Doped Fluorescent Organic Thin Films by Photoluminescence Measurements," *Applied Physics Letters* 96, no. 7 (2010): 073302.

45. M. Flämmich, M. C. Gather, N. Danz, et al., "Orientation of Emissive Dipoles in OLEDs: Quantitative In Situ Analysis," *Organic Electronics* 11, no. 6 (2010): 1039–1046.

46. M. Flämmich, D. Michaelis, and N. Danz, "Accessing OLED Emitter Properties by Radiation Pattern Analyses," *Organic Electronics* 12, no. 1 (2011): 83–91.

47. L. Penninck, P. de Visschere, J. Beeckman, and K. Neyts, "Dipole Radiation Within One-Dimensional Anisotropic Microcavities: A Simulation Method," *Optics Express* 19, no. 19 (2011): 18558–18576.

48. J. A. E. Wasey and W. L. Barnes, "Efficiency of Spontaneous Emission from Planar Microcavities," *Journal of Modern Optics* 47, no. 4 (2000): 725–741.

49. Y. Jin, H. S. Kim, D. Lee, C. Adachi, S. Yoo, and K. Yu, "Rigorous Determination of Dipole Orientation in Organic Thin Films Using Angle-

21951071, 2026, 8, Downloaded from https://advanced.onlinelibrary.wiley.com/doi/10.1002/adom.202600002 by Open Access University of Augsburg - Universitätsbibliothek Augsburg , Wiley Online Library on [23/02/2026]. See the Terms and Conditions (https://onlinelibrary.wiley.com/terms-and-conditions) on Wiley Online Library for rules of use; OA articles are governed by the applicable Creative Commons License

Dependent Photoluminescence," *The Journal of Physical Chemistry C* 128, no. 4 (2024): 1755–1761.

50. M. D. Ediger, J. de Pablo, and L. Yu, "Anisotropic Vapor-Deposited Glasses: Hybrid Organic Solids," *Accounts of Chemical Research* 52, no. 2 (2019): 407–414.

51. S. Cheng, Y. Lee, J. Yu, L. Yu, and M. Ediger, "Surface Equilibration Mechanism Controls the Stability of a Model Codeposited Glass Mixture of Organic Semiconductors," *The Journal of Physical Chemistry Letters* 14, no. 18 (2023): 4297–4303.

52. S. Cheng, Y. Lee, J. Yu, L. Yu, and M. D. Ediger, "Generic Behavior of Ultrastability and Anisotropic Molecular Packing in Codeposited Organic Semiconductor Glass Mixtures," *Chemistry of Materials* 36 (2024): 3205–3214.

53. B. M. Nguyen, M. Schmid, J. Kirsch, A. Cakaj, and W. Brütting, "On the Orientation Mechanism of Nonpolar Dyes in Light-Emitting Guest-Host Systems," *Chemistry of Materials* 35, no. 17 (2023): 7333–7343.

54. C. Scherer, N. Kinaret, K.-H. Lin, et al., "Predicting Molecular Ordering in Deposited Molecular Films," *Advanced Energy Materials* 14, no. 44 (2024): 2403124.

55. T. Morgenstern, M. Schmid, A. Hofmann, M. Bierling, L. Jäger, and W. Brütting, "Correlating Optical and Electrical Dipole Moments to Pinpoint Phosphorescent Dye Alignment in Organic Light-Emitting Diodes," *ACS Applied Materials & Interfaces* 10, no. 37 (2018): 31541–31551.

56. Y. Noguchi, W. Brütting, and H. Ishii, "Spontaneous Orientation Polarization in Organic Light-Emitting Diodes," *Japanese Journal of Applied Physics* 58, no. SF (2019): SF0801.

57. J. S. Bangsund, J. R. van Sambeek, N. M. Concannon, and R. J. Holmes, "Sub-Turn-On Exciton Quenching Due to Molecular Orientation and Polarization in Organic Light-Emitting Devices," *Science Advances* 6, no. 32 (2020): eabb2659.

58. Y. Noguchi, A. Hofmann, and W. Brütting, "Controlling Charge Accumulation Properties of Organic Light-Emitting Diodes Using Dipolar Doping of Hole Transport Layers," *Advanced Optical Materials* 10, no. 21 (2022): 2201278.

59. E. Pakhomenko, S. Martin, S. He, A. Kapur, and R. J. Holmes, "Controlling Polarization-Induced Polaron Accumulation in OLEDs via Device Design," *Advanced Functional Materials* 35 (2024): 2412329.

60. M. K. Callens, D. Yokoyama, and K. Neyts, "Anisotropic Materials in OLEDs for High Outcoupling Efficiency," *Optics Express* 23, no. 16 (2015): 21128–21148.

Supporting Information

Additional supporting information can be found online in the Supporting Information section.

Supporting File: adom70959-sup-0001-SuppMat.pdf.

21951071, 2026, 8, Downloaded from https://advanced.onlinelibrary.wiley.com/doi/10.1002/adom.202600902 by Open Access University of Augsburg - Universitätsbibliothek Augsburg , Wiley Online Library on [23/02/2026]. See the Terms and Conditions (https://onlinelibrary.wiley.com/terms-and-conditions) on Wiley Online Library for rules of use; OA articles are governed by the applicable Creative Commons License